**Engineering and Technology Journal**
**Journal homepage:** engtechjournal.org

# Design and Performance Analysis of Permanent Magnet Synchronous Motor for Electric Vehicles Application

**Mustafa Y. Bdewi [a*], Ahmed M. Mohammed [b], Mohammed M. Ezzaldean [c]**

[a] Electrical Eng. Dept, University of Technology, Baghdad, Iraq. 316539@student.uotechnology.edu.iq

[b] Electrical Eng. Dept., University of Technology, Baghdad, Iraq. 30008@uotechnology.edu.iq

[c] Electrical Eng. Dept, University of Technology, Baghdad, Iraq. 30097@uotechnology.edu.iq

*Corresponding author.

Submitted: 04/07/2020 Accepted: 24/09/2020 Published: 25/03/2021

K E Y W O R D S

Electric vehicle, Finite element method, Permanent magnet synchronous motor, Torque density, Torque ripple.

A B S T R A C T

*In electrical vehicle applications, power density plays a significant role in improving machine performance. The main objective of this paper is to design and analyze the performance of in-wheel outer rotor permanent magnet synchronous motor (PMSM) used in electric vehicles based on a previously designed model. The key challenge is to achieve the best machine performance regarding the highest torque density and lowest torque ripple. This work also aims at reducing the machine cost by using permanent magnet (PM) material, which has less energy density than the PM used in the previously designed model. An optimization procedure is carried out to improve the generated torque, keeping the same aspects of size and volume of the selected machine. On the other hand, the other specifications of the machine are taken into consideration and are maintained within the acceptable level. According to their major impact on the machine's performance, the most important parameters of machine designing is selected during the optimization procedure. This proposed machine is implemented and tested using the finite element software package "MagNet 7.4.1" with Visual Basic 16.0 programming language and MATLAB 9.5 Simulink for post-processing.*

**How to cite this article** M. Y. Bdewi, A. M. Mohammed and M. M. Ezzaldean, "Design and Performance Analysis of Permanent Magnet Synchronous Motor for Electric Vehicles Application," Engineering and Technology Journal, Vol. 39, Part A, No. 03, pp. 394-406, 2021.

DOI: https://doi.org/10.30684/etj.v39i3A.1765

## 1. INTRODUCTION

PMSM is among the most common traction motor kinds in commercially available electric vehicles (EVs) [1]. It has the advantages of high efficiency, low copper losses, evident energy-saving effect, high power density...etc. The magnetic field of the rotor is provided by the PMs, so there are no electrical excitation losses. When the PMSM is in synchronous run time, the electrical losses in the rotor are not present. Moreover, compared with the electrical excited synchronous motors, the rotor structure of the PMSM is simplified considerably. Since this machine does not require electric excitation brushes, the rotating stability of the motor is improved. Having a high produced magnetic energy, the volume of the PM motors can be significantly reduced, which makes them high-density motors [2].

High power/torque density and low torque ripple are among the main requirements for EVs applications [3,4]. There are many factors that cause torque ripple. The harmonic contents in the back EMF and the cogging torque are the main causes of the torque ripple in the permanent magnet motors [5]. This ripple produces vibrations, noise, wearing, and possible mechanical resonances [6]. Thus, PMSM with lower total harmonic distortion (THD) in the EMF and lower torque ripple is related closely to smoother electromagnetic torque.

In [7], the multipolar PMSM with the same number of poles and slots and unequal teeth arrangement was designed. This structure of identical number poles and slots has been used to reduce the inherent cogging torque. The unequal teeth structure was investigated for maximizing the flux linkage of the stator teeth and winding synthesis coefficient and hence maximizing the electromagnetic torque. In [8], the effect of variation of slot opening and rotor pole radius on the cogging torque and the electromagnetic torque of PMSM were analyzed. In [5], the causes of torque ripple of surface-mounted permanent magnet machine were described. Then, the effect of parameters including the shape and magnetization pattern of the permanent magnets, pole span coefficient, eccentricity and slot/pole combination on the harmonic content of back EMF and cogging torque was presented. In [9], the usage of innovative materials such as iron-cobalt (FeCo) and innovative screen printed winding was investigated for increasing the torque density of the permanent magnet machine.

This paper proposes a PMSM with improved torque density based on the initial design using PM material that has less energy density than the PM material used in the initial design keeping the EMF THD and overall torque ripple within an acceptable level. It should be noted that the energy density is one of the PM material characteristics that is equal to the product of its operating flux density and magnetic field strength [10]. The reason for selecting PM with lower energy density is to reduce the overall cost of the proposed machine as it takes the highest share of machine cost. The machine performance improvement is done by selecting an efficient winding topology and optimizing the dimensions, including magnet span, slot opening, and slot width, which have been selected due to their major impact on the PMSM performance. The design and analysis tools are finite element software "MagNet 7.4.1", Visual Basic 16.0, and MATLAB 9.5 Simulink.

This paper is organized as follows: Section 2 presents the numerical modeling. Section 3 describes the machine topology. Section 4 introduces machine optimization. Section 5 shows the results and discussion. Section 6 provides the conclusions.

## 2. NUMERICAL MODELLING

### *I. Electromagnetic field equation*

Sub-domains of PMSM involve permanent magnets, stator, rotor, stator winding, and the air gap. Each one of these has an individual mathematical equation. In general, the electromagnetic field equation of a sub-domain can be written as [11]:

$$\nabla \times (\mu^{-1}(\nabla \times A - B_r)) + \sigma \frac{\partial A}{\partial t} = J - \sigma \nabla \varphi \quad (1)$$

Where, A is the magnetic vector potential, $B_r$ is remnant flux density of magnets, σ is the electric conductivity, $J_s$ is the current density of source, and φ is the electric scalar potential.

For the 2D finite element method (FEM) modeling, as in the case of the studied machine, the end effects are neglected. Therefore, the electric field strength (E), the magnetic vector potential (A) and

the current density ($J_s$) have the only component in the z-direction, so $A = A_z e_z$ , $J = J_z e_z$ and $E = E_z e_z$ Where $e_z$ is the unit vector of z-direction.

***II. Flux linkage and induced voltage***

The flux linkage (ψ) and the induced voltage (e) of a turn can be calculated by FEM as [11]:

$$\psi = \frac{L_c}{S}\iint_{\Omega^+} A_z d\Omega - \iint_{\Omega^-} A_z d\Omega \tag{2}$$

$$e = \frac{L_c}{S}\iint_{\Omega^+} \frac{\partial A_z}{\partial t} d\Omega - \iint_{\Omega^-} \frac{\partial A_z}{\partial t} d\Omega \tag{3}$$

Where $L_c$ is the length of the conductor, $\Omega^+$ and $\Omega^-$ are integration areas corresponding to go and return sides of stator windings equivalent conductors, and S is cross section area of the equivalent conductor.

***III. Electromagnetic torque***

The calculation of the machine's Electromagnetic torque with FEM can be done using Maxwell stress tensor [12]. The formula of this method is written as [13].

$$T = \frac{L_s}{\mu_0}\oint_l r B_n B_t dl \tag{4}$$

Where, $L_s$ is stack length, $l$ is integration contour, $B_n$ is normal magnetic flux density, $B_t$ is tangential magnetic flux density, and r is the circumference radius that lies in the air gap.

***IV. Torque ripple***

In this work, the torque ripple, including cogging torque, is calculated from peak to peak electromagnetic torque. The percentage of torque ripple is calculated using the following formula:

$$T_r = \frac{T_{pp}}{T_{av}} \times 100\% = \frac{T_{max} - T_{min}}{T_{av}} \times 100\% \tag{5}$$

Where Tpp, Tmax, Tmin, Tav are peak to peak torque, maximum torque, minimum torque, and average torque, respectively.

***V. Total harmonic distortion of the air gap flux density***

For calculating the total harmonic distortion of the air gap flux density, spectral analysis by Fast Fourier transform (FFT) using MATLAB 9.5 Simulink will be applied on its data obtained by FEM. The equation for measuring the THD is written as [14]:

$$THD = \frac{\sqrt{\sum_{n=2}^{\infty} B_n^2}}{B_1} \times 100\% \tag{6}$$

Where $B_n$ is $n^{th}$ harmonic components and $B_1$ is the RMS magnitude of the fundamental component of the air gap flux density.

## 3. MACHINE TOPOLOGY

A Machine in EVs can be connected by driveline or directly connected to the wheel. In-wheel motor technology involves fitting a motor in the wheel hub, and the output torque is directly transferred to the wheel, which reduces the retarder, traditional clutch, and other mechanical differentials [15]. The use of in-wheel motors also improves on many aspects of all-wheel drive (AWD) driving systems. Moreover, torque vector control, fast accelerations, higher efficiency, and high ground clearance with a low gravity center design are possible [16]. This type of motor has a restricted size due to its direct connection with the wheel. Traditional electric traction motors have been designed with an internal rotor configuration. The external rotor topology was limited primarily to applications that benefit from having the rotor surface directly connected to the traction drive.

However, electric motors with exterior rotors have been marketed for traditional traction drives in recent years since they provide higher torque compared with internal rotor PMSMs [17].

Considering the topologies above, a pre-designed in-wheel outer rotor PMSM with 72/60 slot-pole combination in [18] has been selected as a working case. Figure 1 shows the general configuration of the proposed machine.

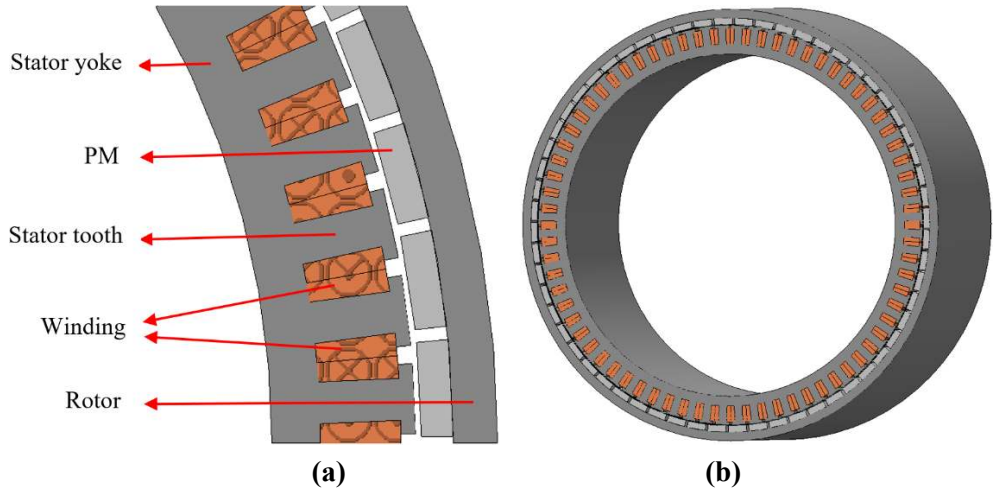


**Figure 1: The Selected PMSM model (a) A sectional view and (b) The overall view**

Neodymium-Iron-Boron (NdFeB) 30/27 PM is used for the selected PMSM. This PM material has less energy density than that used in the reference machine (N38H PM), which is selected for economic concern. The magnetic properties of 30/27 PM type are illustrated in Table I.

**TABLE I: Magnetic specification for the investigated PM materials**

| Parameter | Value |
|---|---|
| Residual flux density | 1.13 T |
| Relative permeability | 1.056 |
| Coercively | -851.72 kA/m |
| Maximum energy density | 240.7 KJ/m$^3$ |

For stator winding, fractional slot concentrated winding (FSCW) is applied. FSCW of PMSMs has acquired a lot of interest in the last few years owing to the advantages provided where a wide constant power range is significant. FSCW has the advantage of improved flux weakening capability, high power density, cost-effective manufacturing, high slot fill factor, short end windings, and high fault tolerance [17]. Reference [19] describes the investigated winding topology that gives a high winding factor for a given slot-pole combination. The winding factor is measured using the induced EMF. The EMF phasor $E_c$ of the conductor (c) and winding factor ($K_w$) are calculated by [19]:

$$E_c = e^{j\frac{\pi.p\ s(c)}{Q_s}} \tag{7}$$

$$K_w = \frac{\sum_{c=1}^{2Q_s/3} E_c}{n_l Q_s/3} \tag{8}$$

Where $Q_s$ presents the slots number, p is the poles number, s indicates the conductors' sequence for one-phase, and $n_l$ is the number of winding layers. Table II shows the calculated winding factors using Eq. (7) and Eq. (8) for double layer concentrated winding with poles number between 42 and 80 and slots number between 45 and 90. For the selected 72 slots/ 60 pole winding configuration, the corresponding winding factor is 0.933.

During the optimization process, the number of turns of the stator winding is set as a variable to ensure that the area of the winding's slots is properly filled with copper, taking into consideration the actual strand area of the slot. Figure 2 illustrates this winding method for a one-sixth section of the selected PMSM, which is symmetric for the other five sections. As it can be seen, the three-phase

winding connection sequence is (A - A'- A'- A - B'- B - B - B'- C - C'- C'- C……) where A', B', C' are the return phases corresponding to phases A, B, C respectively.

**TABLE II: Winding factors for various slot/pole combinations [19]**

| Qs\p | 4 | 6 | 8 | 10 | 12 | 14 | 16 | 18 | 20 | 22 | 24 | 26 | 28 | 30 | 32 | 34 | 36 | 38 | 40 | 42 |
|---|---|---|---|---|---|---|---|---|---|---|---|---|---|---|---|---|---|---|---|---|
| 6 | 0.866 | | 0.866 | 0.500 | | 0.500 | 0.866 | | 0.866 | 0.500 | | 0.500 | 0.866 | | 0.866 | 0.500 | | 0.500 | 0.866 | |
| 9 | 0.617 | 0.866 | | | 0.866 | 0.617 | 0.328 | | 0.328 | 0.617 | 0.866 | | | 0.866 | 0.617 | 0.328 | | 0.328 | 0.617 | 0.866 |
| 12 | 1 | | 0.866 | | | | 0.866 | | … | … | | … | … | | 0.866 | | | | 0.866 | |
| 15 | | | 0.621 | 0.866 | | | | | 0.866 | 0.621 | | … | … | | … | … | | 0.621 | 0.866 | |
| 18 | | 1 | … | 0.647 | 0.866 | | | | | | 0.866 | 0.647 | … | … | … | … | | … | … | … |
| 21 | | | … | … | | 0.866 | 0.890 | | 0.953 | 0.953 | | 0.890 | 0.866 | | … | … | | … | … | |
| 24 | | | 1 | … | | 0.760 | 0.866 | | | 0.950 | | 0.950 | | | 0.866 | 0.760 | | … | … | |
| 27 | | | | … | … | … | … | 0.866 | 0.877 | 0.915 | | 0.954 | 0.954 | | 0.915 | 0.877 | 0.866 | … | … | … |
| 30 | | | | 1 | | … | … | | 0.866 | 0.874 | | 0.936 | | | | 0.936 | | 0.874 | 0.866 | |
| 33 | | | | | | … | … | | … | 0.866 | | 0.903 | 0.928 | | 0.954 | 0.954 | | 0.928 | 0.903 | |
| 36 | | | | | 1 | … | … | | … | … | 0.866 | 0.867 | | | 0.953 | | | 0.953 | | |
| 39 | | | | | | … | … | | … | … | | 0.866 | 0.863 | | 0.918 | 0.936 | | 0.954 | 0.954 | |
| 42 | | | | | | 1 | … | | … | … | | … | 0.866 | | 0.890 | 0.913 | | 0.945 | 0.953 | |

| | | | | | |
|---|---|---|---|---|---|
| 0.866 | $k_{w1}$= 0.866, q=1/2, 1/4 | | $k_{w1}$= 0.945, q=3/8, 3/10 | 0.955 | Qs=21+6k, p=Qs±1, k = 0, 1, 2 … |
| | $k_{w1}$= 0.902, q=3/7, 3/11 | | $k_{w1}$= 0.951, q=5/14, 5/16 | 0.954 | Qs=24+6k, p=Qs±2, k = 0, 1, 2 … |
| | $k_{w1}$= 0.933, q=2/5, 2/7 | | not allowed | … | $k_{w1}$ < 0.866 |

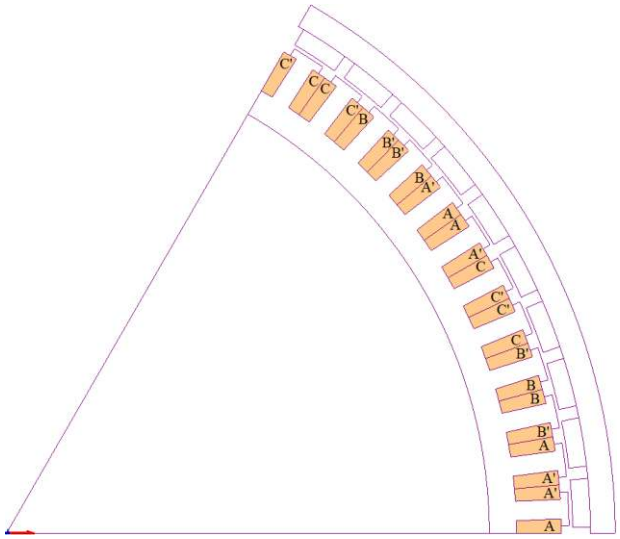


**Figure 2: Winding distribution and configuration of 72/60 slot pole**

## 4. MACHINE OPTIMIZATION

### *I. Optimization tool*

In this work, Visual Basic 16.0 as a script programming tool is coupled with finite element MagNet 7.4.1 software for implementing the design optimization.

The script is a set of instructions comprising executable statements written in a programming language that can be interpreted and executed in another application program by the scripting engine. By using a script:

- Complex and repetitive tasks, including pre-processing and post-processing, can be performed, e.g., parametric modelling, parametric solution, calculation of quantities with the post-processing information and analysis of data.
- The effects of slotting, fringing, and magnetic saturation is considered.
- Smoothly and accurately variation of the model geometry during the optimization process.
- Direct calls to and from other interface compliant software.

Based on the script instructions, MagNet Software creates the machine and edits its dimensions according to the desired specifications. Figure 3 shows how MagNet represents the investigated PMSM using FEM.

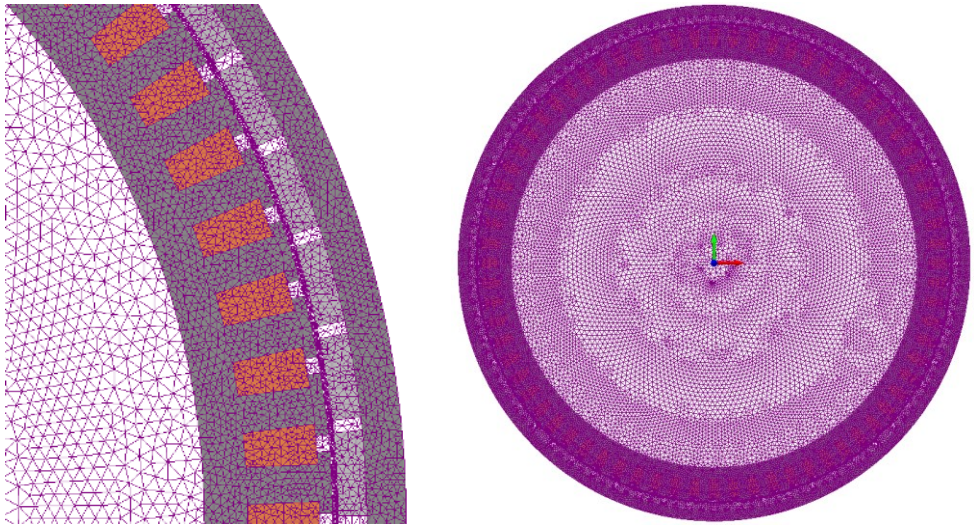

**(a)** **(b)**

**Figure 3: Finite element meshing (a) A sectional view and (b) The overall view**

### *II. Optimization variables*

The selected design variables for optimizing the machine performance are the magnet span, slot opening and slot width. Magnet span is optimized for minimum air gap flux density harmonics and hence minimum EMF THD. Then, slot opening and slot width are optimized for maximum electromagnetic torque and reasonable torque ripple. The design procedure is made at the rated current density of 5 A/mm$^2$ and rated speed of 500 rpm. The design variables and their ranges are illustrated in Figure 4 and Table III.

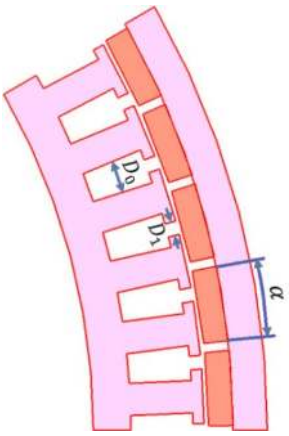


**Figure 4: Design variables of the studied machine**

**TABLE III: Design variables range for the studied machine**

| Parameter | Range |
|---|---|
| Slot Width ($D_0$) | ≥10 mm |
| Slot Opening ($D_1$) | 20% - 80% |
| Magnet Span (α) | 30% - 100% |

The following notifications about the table:

- Variable design parameters have been chosen as they have a major effect on machine performance.

- The term magnet span is defined as the percentage of the rotor area that is covered by one magnet. For illustration, Figure 5 displays sections of a rotor with different magnet span.
- Slot opening means the percentage of slot ending opened by tooth tip. Figure 6 shows sections of a stator with a different slot opening.
- The upper limit and lower limit of slot opening is set to avoid high leakage flux by PMs.
- The lower limit of magnet span is set to avoid low magnetic field density.
- The slot width is set to be close to tooth width or wider. The wider slot width, the higher number of turns per coil, and hence higher electromagnetic torque. The upper limit of slot width is constrained by magnetic circuit saturation and mechanical strength.

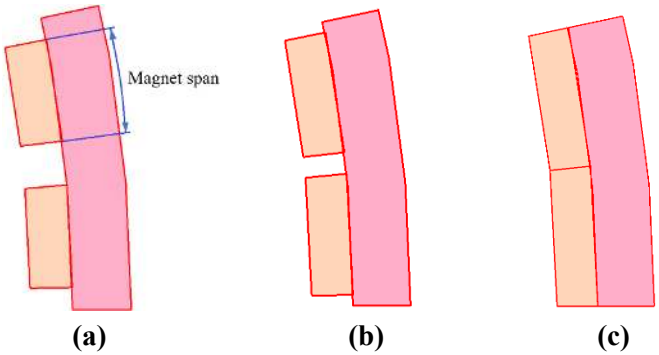


**Figure 5: A PMSM's rotor section with different mahnet span (a- 70% b- 85% and c- 100%)**

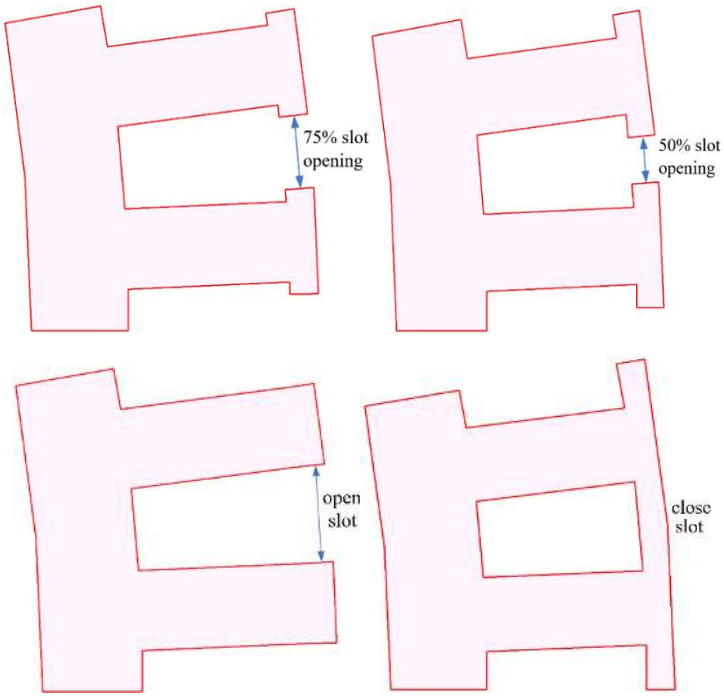


**Figure 6: Two teeth of a PMSM with a different slot opening**

## 5. Results and Discussion

### *I. Minimization of the THD of air-gap flux density*

In this section, the effect of magnet span on THD of air-gap flux density is simulated and analyzed. The simulation is made under the condition of no slot opening or, in other words, "without slots in the stator" in order to remove any other effects on the magnet flux distribution. The aim of the analysis is to obtain the optimum magnet span with less THD in the air gap flux density and hence less EMF waveforms harmonic content.

Figure 7 shows the variation of THD of the air gap flux density as a function of magnet span. It can be observed that the THD is decreasing with magnet span, reaching minimum value of 13.19% at

magnet span of 70%. With higher ratio, it starts increasing for the most rest of magnet span. The selected optimum point will be 70% magnet span because it has lowest THD. Figure 8 shows the air gap flux density distribution with different magnet span at the condition of closed slots. The maximum value is kept constant by maintaining PM height to avoid the high saturation level in the machine iron core.

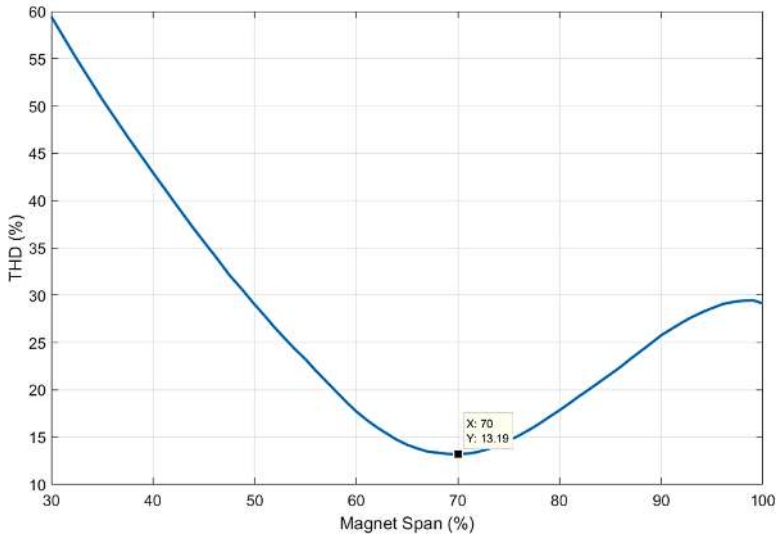


**Figure 7: THD variation of air-gap flux density as a function of magnet span**

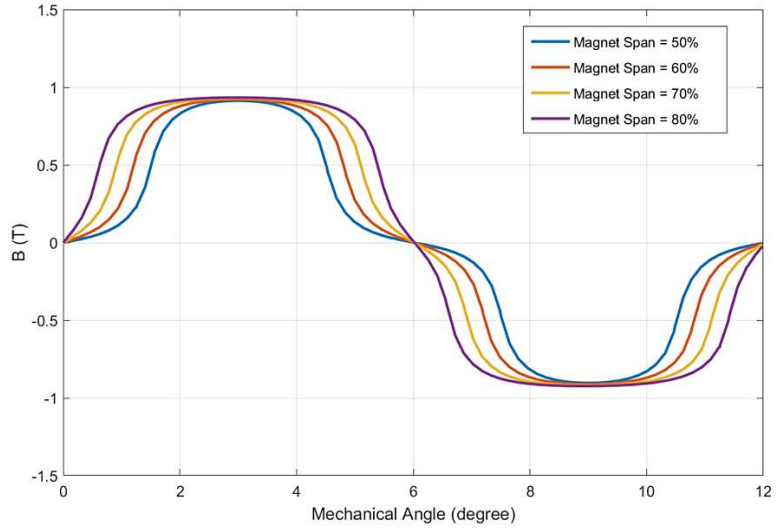


**Figure 8: Air gap flux density waveforms for different magnet span at closed slot**

### *II. Electromagnetic torque and torque ripple optimizations*

In this section, the influence of slot opening and slot width on the electromagnetic torque and torque ripple is investigated. Slot opening and slot width are optimized for the aim of maximizing the electromagnetic torque and minimizing torque ripple using the optimum magnet span obtained in the previous section.

Figure 9 presents mean torque as a function of slot opening and slot width. It can be seen that the average torque has the maximum value at the coordinates (slot opening (%), slot width (mm), electromagnetic torque (Nm)) = (40, 14, 1585.162). However, when the slot width is greater than 12.5 mm, the machine teeth will be saturated (tested by the simulation). Therefore, it is not possible to select the design with a slot width greater than this value. From this analysis, the optimum electromagnetic torque corresponds to the coordinates = (32, 12.5, 1551.483).

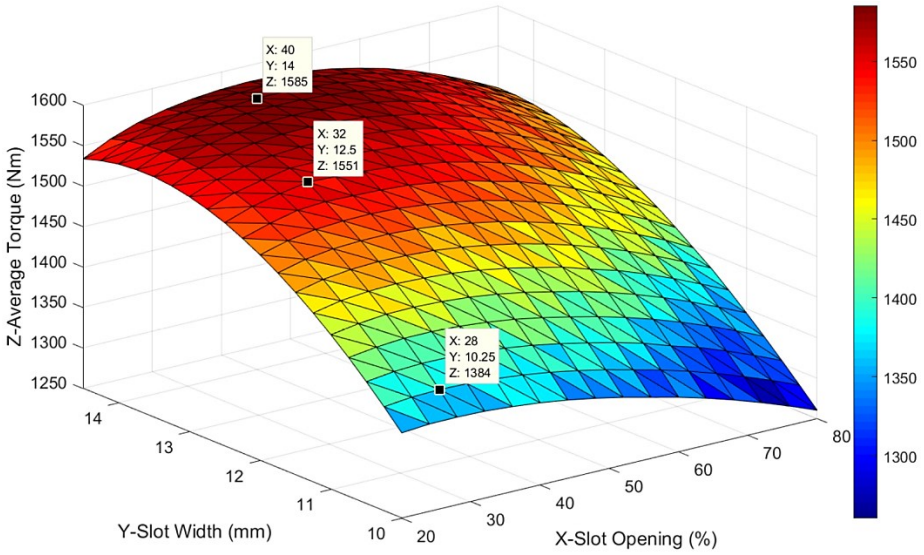


**Figure 9: Electromagnetic torque as a function of slot opening and slot width**

Figure 10 presents the torque ripple variation with respect to slot opening and slot width. It can be observed that torque ripple's smallest value is at coordinates = (28%, 10.25mm, 1.082%). Meanwhile, at those optimum parameters of minimum torque ripple, average torque only reaches 1383.651 Nm that is significantly smaller than the optimal torque of 1551.483 Nm. In the case of optimum electromagnetic torque point, the torque ripple equal to 3.902%.

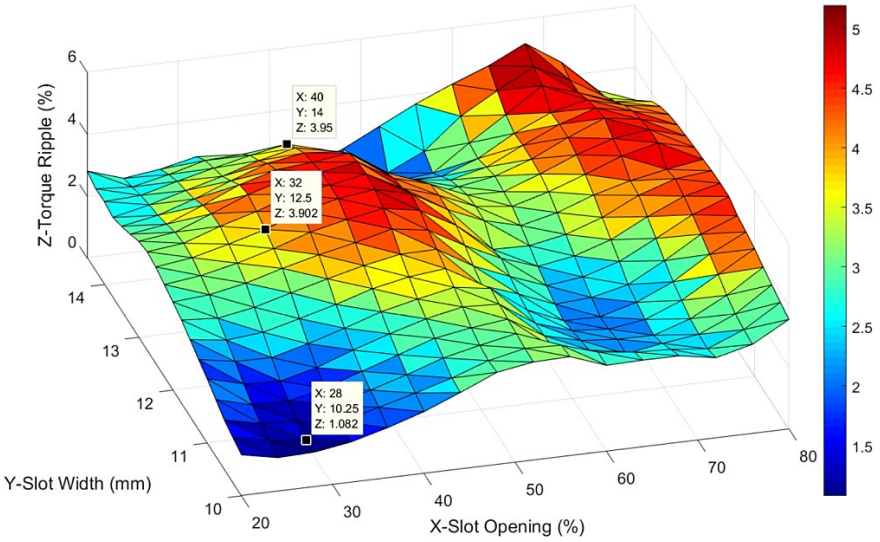


**Figure 10: Torque ripple as a function of slot opening and slot width**

From this analysis, the selected point has 32% slot opening and 12.5 mm slot width. The reason for choosing this point is that it has high electromagnetic torque and low torque ripple. Table IV compares the magnet span, slot opening, and slot width for the existed and designed model.

**TABLE IV:Design dimensions for the proposed and existed PMSM**

| Machine geometry parameters | Designed PMSM | Existed PMSM |
|---|---|---|
| Magnet span (%) | 70 | 88.4 |
| Slot opening (%) | 32 | 39.2 |
| Slot width (mm) | 12.5 | 10.4 |

### *III. Magnetic flux density and flux lines distribution*

Figure 11 shows the flux density distribution and the contour of flux lines that link the stator and rotor of the proposed machine.

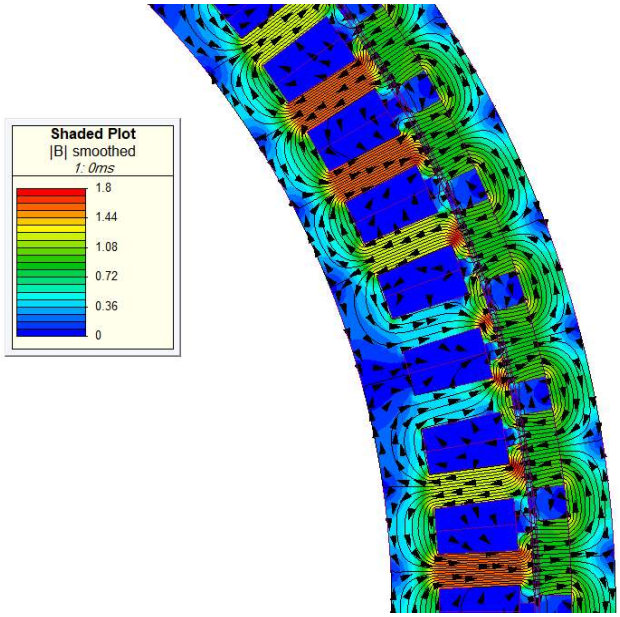


**Figure 11: Flux density and flux lines distribution for a section of the proposed PMSM**

### *IV. Back EMF characteristics*

The induced EMF waveforms and their harmonic spectrums of the designed and existed machines at 500 rpm speed are shown in Figure 12 and Figure 13, respectively. From the harmonic spectrums, it can be seen that the 5$^{th}$, 9$^{th}$ and 11$^{th}$ harmonics of the proposed PMSM have a higher magnitude than that of the existed PMSM. However, each one of these harmonics has a value below 1% of the RMS fundamental component of the EMF causing only a slight increase in the THD that does not affect the overall machine performance. The calculated THD for the pre-designed PMSM is equal to 2.83% and that for proposed PMSM is equal to 2.94%.

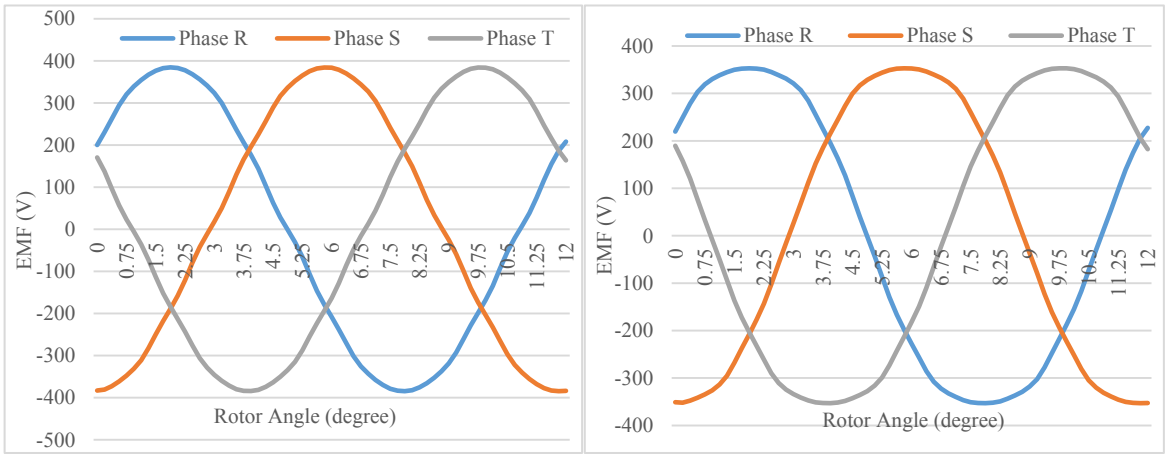


**Figure 12: EMF waveforms of the (a) Designed PMSM and (b) Existed PMSM**

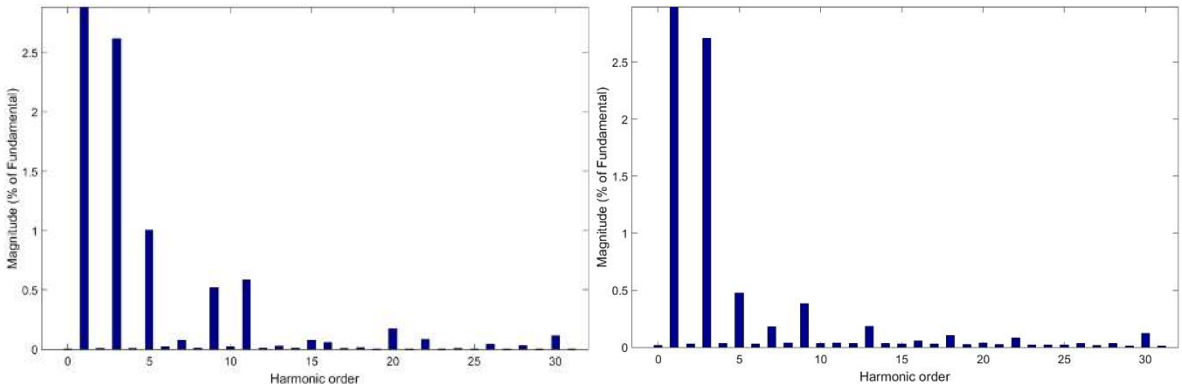


**(a)** **(b)**

**Figure 13: EMF Harmonic spectrum of the (a) Designed PMSM and (b) Existed PMSM**

### *V. Torque density and torque ripple characteristics*

The electromagnetic torque variation as a function of rotor angle for the designed and pre-designed PMSM is shown in Figure 14. The simulation is done at the rated current density and at rated speed. The characteristics which can be concluded from the figure are summarized in Table V.

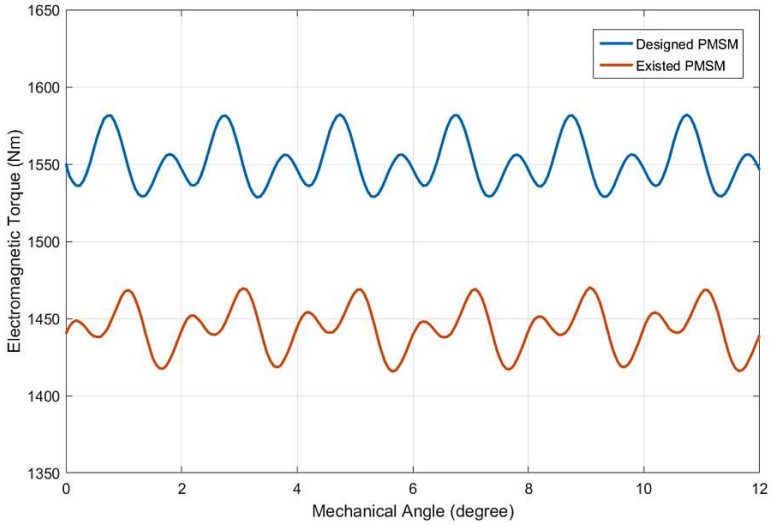


**Figure 14: Electromagnetic torque variation with respect to rotor mechanical angle**

**TABLE V: Electromagnetic torque characteristics of the designed and existed PMSM**

| Parameters | Designed PMSM | Existed PMSM |
|---|---|---|
| Average Torque (Nm) | 1551.483 | 1443.612 |
| Torque density (Nm/Kg) | 10.122 | 9.137 |
| Peak to peak torque ripple (Nm) | 60.541 | 54.265 |
| Torque ripple (%) | 3.902 | 3.759 |

To confirm the validity of the designed machine, Table VI compares the existed and designed model in terms of electromagnetic torque, torque density, torque ripple, and EMF THD for various current densities and speeds. It can be seen that the designed machine has higher average torque than a pre-designed machine. THD and torque ripple are almost the same for both machines, and THD does not change for various operating points.

**TABLE VI:Comparison between the existed and designed PMSM**

| | | Existed PMSM | New designed PMSM |
|---|---|---|---|
| ***Operating Point (1) Current = 3 A/mm$^2$ Speed = 500 rpm*** | Electromagnetic Torque (Nm) | 858.462 | 934.295 |
| | Torque density (Nm/ Kg) | 5.433 | 6.096 |
| | Torque ripple (%) | 4.372 | 4.254 |
| | THD (%) | 2.83% | 2.94% |
| ***Operating Point (2) Current = 7 A/mm$^2$ Speed = 400 rpm*** | Electromagnetic Torque (Nm) | 1967.093 | 2139.852 |
| | Torque density (Nm/ Kg) | 12.45 | 13.961 |
| | Torque ripple (%) | 3.098 | 3.315 |
| | THD (%) | 2.83% | 2.94% |
| ***Operating Point (3) Current = 11 A/mm$^2$ Speed = 300 rpm*** | Electromagnetic Torque (Nm) | 3042.025 | 3263.761 |
| | Torque density (Nm/ Kg) | 19.253 | 21.294 |
| | Torque ripple (%) | 2.454 | 2.471 |
| | THD (%) | 2.83% | 2.94% |
| ***Operating Point (4) Current = 15 A/mm$^2$ Speed = 200 rpm*** | Electromagnetic Torque (Nm) | 4082.852 | 4278.117 |
| | Torque density (Nm/ Kg) | 25.841 | 27.912 |
| | Torque ripple (%) | 2.218 | 2.553 |
| | THD (%) | 2.83% | 2.94% |

## 6. CONCLUSION

This paper presents a new design of in-wheel, outer rotor PMSM. In order to achieve the desired performance level, fractional slot concentrated winding topology was used for the stator winding due to its advantages. For the machine optimization, the parameters including magnet span, slot opening and slot width were selected due to their significant effect on the machine performance. The magnet span was firstly optimized for minimum EMF THD. Then, slot width and slot opening were optimized for maximum electromagnetic torque and acceptable torque ripple using the optimum magnet span. This investigated machine was implemented and tested using finite element software "MagNet 7.4.1" with Visual Basic 16.0 as a programming tool and MATLAB 9.5 Simulink for post-processing. At the rated current density and speed, the electromagnetic torque and torque density for the designed PMSM are 1551.483 Nm and 10.122 Nm/Kg, respectively, while that for existed PMSM are 1443.612 Nm and 9.137 Nm/Kg, respectively. The results show that the required specification for the investigated PMSM has been improved from electromagnetic torque and torque density perspective, and the torque ripple and THD have been kept almost the same compared with the existing motor design. Also, the cost of the designed machine has been reduced by replacing the PM material type that is used in the existing machine with neodymium iron boron: 30/27 PM, and reducing the magnet span from 88.4% to 70%.

## References

**[1]** V. Ruuskanen, J. Nerg, J. Pyrhönen, S. Ruotsalainen and R. Kennel, "Drive Cycle Analysis of a Permanent-Magnet Traction Motor Based on Magnetostatic Finite-Element Analysis," IEEE Transactions on Vehicular Technology, vol. 64, no. 3, pp. 1249-1254, March 2015.

**[2]** L. Wang, X. Deng, J. Lu, K. Wang and R. Wang, "Design and Finite Element Analysis of Permanent Magnet Synchronous Motor with Novel Rotor Type," Asia-Pacific Power and Energy Engineering Conference, Chengdu, pp. 1-4, 2010.

**[3]** Y. Zhang, W. P. Cao and J. Morrow, "Interior permanent magnet motor parameter and torque ripple analysis for EV traction," IEEE International Conference on Applied Superconductivity and Electromagnetic Devices (ASEMD), Shanghai, pp. 386-387, 2015.

**[4]** G. J. Li, B. Ren and Z. Q. Zhu, "Cogging torque and torque ripple reduction of modular permanent magnet machines," International Conference on Electrical Machines (ICEM), Lausanne, pp. 193-199, 2016.

**[5]** S. Huang, J. Zhang, J. Gao and K. Huang, "Optimization the Electromagnetic Torque Ripple of Permanent Magnet Synchronous Motor," International Conference on Electrical and Control Engineering, Wuhan, pp. 3969-3972, 2010.

**[6]** S. Rojas, M. A. Pérez, J. Rodríguez and H. Zelaya, "Torque ripple modeling of a permanent magnet synchronous motor," IEEE International Conference on Industrial Technology, Vina del Mar, pp. 433-438, 2010.

**[7]** Jiakuan Xia, Ting Dong, Chengyuan Wang and Jianyu Zhao, "Low speed high torque PMSM design based on unequal teeth structure," International Conference on Electrical Machines and Systems, Wuhan, pp. 3274-3277, 2008.

**[8]** J. A. Güemes, P. M. García, A. M. Iraolagoitia, and J. J. Ugartemendia, "Influence of slot opening width and rotor pole radius on the torque of PMSM," Renewable Energy & Power Quality Journal, vol. 1, no. 7, pp. 876–880, 2009.

**[9]** M. Lindner, P. Bräuer and R. Werner, "Increasing the torque density of permanent-magnet synchronous machines using innovative materials and winding technologies," *International Multi-Conference on Systems, Signals & Devices*, Chemnitz, pp. 1-7, 2012.

**[10]** R. Krishnan, "Permanent Magnet Synchronous and Brushless DC Motor Drives," CRC press, 1st ed., Boca Raton, 2010.

**[11]** H. V. Xuan, D. Lahaye, M. J. Hoeijmakers, H. Polinder and J. A. Ferreira, "Modeling magnetic saturation for the design of exterior rotor permanent magnet machines," International Power Electronics Conference - ECCE ASIA -, Sapporo, pp. 1299-1305, 2010.

**[12]** J. Pyrhönen, T. Jokinen, and V. Hrabovcová, "Design of rotating electrical machines," John Wiley & Sons, 2nd ed., Chichester, 2008.

**[13]** J. A. Güemes, A. M. Iraolagoitia, M. P. Donsion and J. I. Del Hoyo, "Analysis of torque in permanent magnet synchronous motors with fractional slot windings," International Conference on Electrical Machines, Vilamoura, pp. 1-4, 2008.

**[14]** Y. Li, J. Xing, T. Wang and Y. Lu, "Programmable Design of Magnet Shape for Permanent-Magnet Synchronous Motors with Sinusoidal Back EMF Waveforms," IEEE Transactions on Magnetics, vol. 44, no. 9, pp. 2163-2167, Sept. 2008.

**[15]** Y. Zhou, S. Li, Z. Fang and Q. Zhou, "Control strategy for ABS of EV with independently controlled four in-wheel motors," IEEE Conference on Industrial Electronics and Applications, Xi'an, pp. 2471-2476, 2009.

**[16]** O. Côté, A. Chebak and J. Méthot, "Design and Optimization of a high torque in-wheel surface-mounted PM synchronous motor using concentrated winding," International Electric Machines & Drives Conference, Illinois, pp. 863-870, 2013.

**[17]** A. Tovar-Barranco, F. Briz, A. López-de-Heredia and I. Villar, "Comparison of permanent magnet synchronous machines with concentrated windings and different rotor configurations," European Conference on Power Electronics and Applications (EPE'17 ECCE Europe), Warsaw, pp. 1-8, 2017.

**[18]** S. Bandyopadhyay, "Design Optimization of Surface Mounted Permanent Magnet Synchronous Motors for In-wheel Electric Vehicle Applications," M.Sc. Thesis, DC systems, Energy conversion & Storage Dept., Delft Univ. of Technology, Delft, Netherlands, 2015.

**[19]** F. Libert, and J. Soulard, "Investigation on pole-slot combinations for permanent-magnet machines with concentrated windings," International Conference on Electrical Machines (ICEM), pp. 530-535, 2004.